Planar Near-Field Scanning in the Time Domain, Part 2: Sampling Theorems and Computation Schemes

Thorkild B. Hansen, *Member, IEEE*, and Arthur D. Yaghjian, *Fellow, IEEE*

Abstract— **In Part 1 of this work planar near-field measurements were formulated in the time domain for acoustic and electromagnetic fields. In this paper (Part 2), two computation schemes for calculating the far-field pattern in the time domain from sampled near-field data are developed and applied. The sampled near-field data consists of the values of the field on the scan plane measured at discrete times and at discrete points on the scan plane. The first computation scheme is based on a frequency-domain near-field to far-field formula and applies frequency-domain sampling theorems to the computed frequency-domain near field. The second computation scheme is based on a time-domain near-field to far-field formula and computes the time-domain far field directly from the time-domain near field. A time-domain sampling theorem is derived to determine the spacing between sample points on the scan plane. The computer time for each of the two schemes is determined and numerical examples illustrate the use and the general properties of the schemes. For large antennas the frequency-domain computation scheme takes less time to compute the full far field than the time-domain computation scheme. However, the time-domain computation scheme is simpler, more direct, and easier to program. It is also found that planar time-domain near-field antenna measurements, unlike single-frequency near-field measurements, have the capability of eliminating the error caused by the finite scan plane, and thus can be applied to broadbeam antennas.**

I. Introduction and Summary of Results

THIS paper is the second part of a series of two papers on the subject of time-domain planar near-field scanning. The first paper [1] derived the necessary formulas for calculating acoustic or electromagnetic fields in a half space in terms of their values on a plane. This paper derives sampling theorems and presents two different computation schemes to numerically calculate the time-domain far-field pattern from sampled time-domain near-field data. The sampled time-domain near-field data is obtained by measuring the near-field at discrete points on a finite scan plane at discrete times. We derive sampling theorems and present computation schemes for the corresponding probe-corrected time-domain planar near-field formulas in the report [2]. This work on probe correction has recently been submitted for publication [3].

The first scheme of this paper, called the frequency-domain computation scheme, is based on the frequency-domain formulation in [1, sec. 2]. This frequency-domain scheme consists of the following three steps: 1) use the Fourier transform to calculate the frequency-domain near field from the time-domain near field, 2) calculate the frequency-domain far field from the frequency-domain near field, and 3) use the inverse Fourier transform to calculate the time-domain far field from the frequency-domain far field. This scheme makes use of well-known frequency-domain far-field formulas, sampling theorems, and the fast Fourier transform (FFT).

The second scheme, called the time-domain computation scheme, is based on the time-domain formulation in [1, sec. 3]. This time-domain scheme simply uses the formula that directly gives the time-domain far field in terms of the time-domain near field. A time-domain sampling theorem is derived to determine how small the sample spacing between points on the scan plane has to be in order to calculate the far field accurately.

The use of the two computation schemes is illustrated by calculating the time-domain far-field pattern of a simple acoustic point-source antenna from sampled near-field values taken on a finite scan plane.

The time-domain computation scheme is much simpler to program and use than the frequency-domain computation scheme. However, because the frequency-domain computation scheme uses the FFT it is much faster for large antennas than the time-domain computation scheme when the full far field is calculated for all times. When only part of the far field is calculated, the difference in computer time for the two computation schemes becomes smaller and the time-domain computation scheme therefore becomes more advantageous because of its simplicity. Furthermore, the time-domain computation scheme has the capability of being able to calculate the far-field pattern at early times from near-field measurements taken at early times only. This capability is not possessed by the frequency-domain computation scheme because the near field is required for its entire duration to calculate its Fourier transform.

For many antennas fed by short pulses, the time dependence of both the near field and far field consists of an early-time part, which contains most of the power, and a late-time part, which is oscillatory and contains little power. The duration of the early-time part may be much smaller than the duration of the entire field. If only the early-time part of the far field is of interest, one can use the time-domain computation scheme to determine this part from near-field measurements taken for early times only. Thereby one can significantly reduce

Manuscript received November 22, 1993; revised May 13, 1994. This work was supported by the National Research Council, Washington, DC; by the Danish Technical Research Council, Copenhagen, Denmark; and by the Air Force Office of Scientific Research, Bolling AFB, DC.

The authors are with Rome Laboratory ERCT, 31 Grenier Street, Hanscom AFB, 01731-3010 MA USA

IEEE Log Number 9404566.

U.S. Government work not protected by U.S. copyright

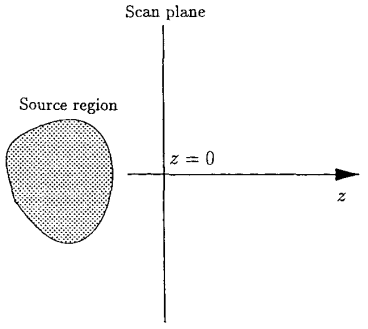

Fig. 1. Planar scanning geometry.

the number of near-field time samples needed for the far-field calculation. If instead the frequency-domain computation scheme is used, the number of near-field time samples cannot be reduced because time samples taken over the entire duration of the near field are needed.

For both schemes, the duration of the computed far-field pattern is extended erroneously due to the finite-size scan plane, and this longer time duration has to be taken into account in the frequency-domain calculation scheme. Specifically, the frequency spacing in the frequency-domain computation scheme must be chosen small enough so that significant time-domain aliasing is avoided in the calculation of the time-domain far-field pattern. The problem of choosing the frequency spacing small enough does not occur for the time-domain computation scheme because no frequency spacing is used.

No matter which scheme is chosen, planar time-domain near-field antenna measurements can eliminate the error in the far-field pattern due to the finite scan plane because this error is separated in time from the correct far-field pattern. This makes it possible to use planar scanning in the time domain to compute the far field of broadbeam antennas in both the time and frequency domains.

II. A Time-Domain Sampling Theorem and Numerical Far-Field Calculations

The geometry under consideration is shown in Fig. 1, where the arbitrary finite source region is located in the half space $z < 0$ and the values of the fields are measured on the plane $z = 0$. The part of space not occupied by the sources is lossless free space with permeability μ and permittivity ϵ. In addition to the rectangular coordinates (x, y, z), the usual spherical coordinates (r, θ, ϕ) defined by $x = r\cos\phi\sin\theta$, $y = r\sin\phi\sin\theta$, and $z = r\cos\theta$ will be used. Throughout the paper $e^{-i\omega t}$ time dependence is suppressed in all the time-harmonic equations.

The first scheme, which is presented in part A of this section, is based on the frequency-domain formulation of [1, sec. 2.3], and the second scheme, which is presented in part B, is based on the time-domain formulation of [1, sec. 3.3] and on a time-domain sampling theorem that will be derived in this section.

In part C, the two computation schemes are compared and used to calculate the far-field pattern of a simple acoustic point-source antenna from near-field data. The reason for illustrating the use of the two computation schemes with an acoustic point-source antenna is that its near field is given by a simple closed-form scalar expression that is easy to compute. Although this acoustic point-source antenna is very simple, it illustrates the general properties of the two computation schemes very well. For different types of antennas we also compare the convenience and the computer time of the two computation schemes. Most of the formulas of this section are derived for electromagnetic fields, and the corresponding results for the acoustic fields are very similar and can be found in [4, ch. 4].

A. Frequency-Domain Computation Scheme

The frequency-domain computation scheme consists of first calculating the frequency-domain near field by taking the Fourier transform of the measured time-domain near field

$$\hat{z} \times \bar{E}_\omega(\bar{r}_0) = \frac{1}{2\pi}\int_{-\infty}^{+\infty} \hat{z} \times \bar{E}(\bar{r}_0, t)e^{i\omega t}dt, \quad \bar{r}_0 = x_0\hat{x} + y_0\hat{y} \tag{1}$$

and then using the frequency-domain far-field formula [1, (17)] to get the frequency-domain far-field pattern

$$\bar{\mathcal{F}}_\omega(\theta, \phi) = \frac{i\omega}{2\pi c}\hat{r} \times \int_{-\infty}^{+\infty}\int_{-\infty}^{+\infty} \hat{z} \times \bar{E}_\omega(\bar{r}_0)e^{-i\omega\hat{r}\cdot\bar{r}_0/c}dx_0dy_0. \tag{2}$$

The time-domain far-field pattern is then found by Fourier transforming the frequency-domain far-field pattern

$$\bar{\mathcal{F}}(\theta, \phi, t) = \int_{-\infty}^{+\infty} \bar{\mathcal{F}}_\omega(\theta, \phi)e^{-i\omega t}d\omega. \tag{3}$$

We will now show how the integrals (1)–(3) can be calculated using the fast Fourier transform (FFT).

If the time-domain near field is effectively bandlimited, such that $\bar{E}_\omega$ can be set equal to zero for $|\omega| > \omega_{max}$, the sampling theorem [5, sec. 5.4] can be applied to convert (1) to the summation

$$\hat{z} \times \bar{E}_\omega(\bar{r}_0) = \frac{1}{2\pi}\sum_{m=-\infty}^{+\infty} \hat{z} \times \bar{E}(\bar{r}_0, m\Delta t)e^{i\omega m\Delta t}\Delta t, \quad |\omega| < \omega_{max} \tag{4}$$

where $\Delta t = \pi/\omega_{max}$ is the time sample spacing determined from the sampling theorem. In practice, the time signal begins at some time t_0 (which may depend on the position in the scan plane) and ends approximately at some time that can be expressed as $t_0 + (N_\omega - 1)\Delta t$. Then (4) can be written as

$$\hat{z} \times \bar{E}_\omega(\bar{r}_0) = \frac{1}{2\pi}\sum_{m=0}^{N_\omega - 1} \hat{z} \times \bar{E}(\bar{r}_0, t_0 + m\Delta t)e^{i\omega(t_0 + m\Delta t)}\Delta t, \quad |\omega| < \omega_{max}\,. \tag{5}$$

According to Nussbaumer [6, p. 88], if N_ω is chosen such that $N_\omega = 2^I$, where I is an integer, the FFT requires $M = \frac{1}{2}N_\omega\log_2(N_\omega)$ complex multiplications and $A = N_\omega\log_2(N_\omega)$ complex additions to calculate (5) for the following N_ω values of ω: $\omega = n\Delta\omega$, $n = 0, 1, 2, \cdots, N_\omega - 1$ with $\Delta\omega = 2\omega_{max}/N_\omega$. (There appears to be no significant reduction in the number of complex multiplications if $\bar{E}_\omega$ is

calculated only for $n = 0$ to $n = N_\omega/2$.) Since complex multiplications takes considerably longer than complex additions, the required computer time is approximately proportional to $M = \frac{1}{2}N_\omega \log_2(N_\omega)$.

Having calculated the frequency-domain near field, we can now use (2) and the two-dimensional FFT to calculate the frequency-domain far-field pattern. According to the frequency-domain sampling theory [7, Fig. 10], one must sample the near field (outside the reactive zone of the radiator) with a sample spacing of approximately $\Delta x_0 = \Delta y_0 = \lambda_{min}/2$, where $\lambda_{min} = 2\pi c/\omega_{max}$ is the minimum effective wavelength occurring in the time-domain field. The double integral in (2) is thereby replaced by an infinite double summation. For actual measurements, the scan area is finite and the infinite double summation is given by

$$\bar{\mathcal{F}}_\omega(\theta,\phi) = \frac{i\omega}{2\pi c}\hat{r} \times \sum_{m=-N_x}^{N_x}\sum_{n=-N_y}^{N_y} \hat{z} \times \bar{E}_\omega(\bar{r}_{0mn})e^{-i\omega\hat{r}\cdot\bar{r}_{0mn}/c}\Delta x_0 \Delta y_0 \quad (6)$$

where $\bar{r}_{0mn} = m\Delta x_0\hat{x} + n\Delta y_0\hat{y}$ is a sampling point on the scan plane. The integers N_x and N_y are determined by the size of the scan plane and are proportional to $k_{max}r_s$, where $k_{max} = 2\pi/\lambda_{min} = \omega_{max}/c$ and r_s is the radius of the circle circumscribing the scan plane.

From [6, p. 103] the number of complex multiplications it takes for the two-dimensional FFT to calculate the full far-field pattern (6) for a fixed ω at $4N_xN_y$ far-field points is $M = 2N_xN_y \log_2(4N_xN_y)$, which is proportional to $(k_{max}r_s)^2 \log_2(k_{max}r_s)$. (Again it is assumed that N_x and N_y are chosen equal to 2 raised to an integer.) If we are interested only in a single principal-plane far-field cut ($\phi = 0$ or $90°$), the number of operations for large scan planes is dominated by the $4N_xN_y$ complex additions needed to collapse [8] the data in one of the rectangular coordinates before performing the FFT in the remaining rectangular coordinate. Thus the number of operations required to compute the far field in a principal plane is proportional to $(k_{max}r_s)^2$.

Now that the frequency-domain far-field pattern is calculated, (3) can be used to calculate the time-domain far-field pattern. The integral in (3) is converted to

$$\bar{\mathcal{F}}(\theta,\phi,t) = \sum_{m=-N_\omega/2}^{N_\omega/2} \bar{\mathcal{F}}_{m\Delta\omega}(\theta,\phi)e^{-im\Delta\omega t}\Delta\omega, \qquad \Delta\omega = \frac{2\omega_{max}}{N_\omega} \quad (7)$$

by means of the sampling theorem if the far field $\bar{\mathcal{F}}(\theta,\phi,t)$ has about the same duration as the near field $\bar{E}(\bar{r}_0,t)$. The values of $\bar{\mathcal{F}}_\omega$ for negative ω is obtained from the equation $\bar{\mathcal{F}}_\omega = \bar{\mathcal{F}}^*_{-\omega}$, where $*$ indicates complex conjugation. If the time duration of the far field is longer than that of the near field, one must decrease the frequency sample spacing $\Delta\omega$ (by increasing N_ω in the FFT's used to compute (5) and (7)) to avoid significant time-domain aliasing. Specifically, if the duration of the far field is T_f, the frequency sample spacing $\Delta\omega$ should be chosen less than or equal to $2\pi/T_f$ according to the sampling theorem. (This is seen by shifting the far-field pattern such that it is symmetric around $t = 0$ and then noting that the shifted far-field pattern is zero for $|t| > \frac{1}{2}T_f$. In part C of this section, it will be shown that T_f, in general, depends not only on the near field but also on the size of the scan plane. The reason for this is that the artificial edges of the scan plane produce a diffracted field, which will make the time duration of the far-field pattern calculated from (6) longer than that of the exact far-field pattern. In the frequency domain, this diffracted field produced by the artificial edges of the finite scan plane cannot be separated from the true radiated fields. For broadbeam antennas, this finite scan-plane error can be large enough to prevent the accurate determination of their radiation patterns from frequency-domain planar near-field measurements [9] (see Part C). The FFT calculation of the summation (7) for N_ω different values of t requires $M = \frac{1}{2}N_\omega \log_2(N_\omega)$ complex multiplications.

Let us now calculate the total number of complex multiplications required for the computation of the full time-domain far-field pattern at $4N_xN_y$ different angles of observation and N_ω different times. To calculate the frequency-domain near field from the summation (5) for $4N_xN_y$ near-field points and for N_ω different frequencies requires $M_1 = 2N_xN_yN_\omega \log_2(N_\omega)$ complex multiplications. Furthermore, to calculate the frequency-domain far-field pattern from (6) for $4N_xN_y$ different angles of observation and N_ω different frequencies requires $M_2 = 2N_xN_yN_\omega \log_2(4N_xN_y)$ complex multiplications. Finally, to calculate the time-domain far-field pattern from (7) for $4N_xN_y$ different angles of observation and N_ω different times requires $M_3 = 2N_xN_yN_\omega \log_2(N_\omega)$ complex multiplications. Consequently, the total number of complex multiplications required for this FFT computation of the full far field is

$$\begin{aligned} M_f &= M_1 + M_2 + M_3 \\ &= N_xN_yN_\omega[4\log_2(N_\omega) + 2\log_2(4N_xN_y)] \\ &\sim (k_{max}r_s)^2N_\omega[\log_2(N_\omega) + \log_2(k_{max}r_s)]. \end{aligned} \quad (8)$$

Similarly, the number of operations required to calculate a principal-plane far-field cut (for example, the $\phi = 0$ cut) at N_ω different times is dominated by the

$$M_c = M_1 = 2N_xN_yN_\omega \log_2(N_\omega) \sim (k_{max}r_s)^2N_\omega \log_2(N_\omega) \quad (9)$$

complex multiplications required to calculate the frequency-domain near field at $4N_xN_y$ near-field points and N_ω different frequencies.

Part C of this section shows a numerical example that illustrates the use of the frequency-domain computation scheme and discusses some of its advantages and disadvantages. The formulas for the acoustic field can be obtained from the formulas of this section by replacing $\hat{z} \times \bar{E}$ with Φ, $\bar{\mathcal{F}}$ with $\mathcal{F}$, and $\hat{r}\times$ with $-\cos\theta$, respectively. Having explained the frequency-domain computation scheme, the next part deals with the time-domain computation scheme.

B. Time-Domain Computation Scheme

The time-domain computation scheme consists simply of using the direct time-domain formula [1, (77)] for the far-field

pattern

$$\bar{\mathcal{F}}(\theta,\phi,t) = -\frac{1}{2\pi c}\hat{r}\times\int_{-\infty}^{+\infty}\int_{-\infty}^{+\infty}\hat{z} \times\frac{\partial}{\partial t}\bar{E}(\bar{r}_0, t+\hat{r}\cdot\bar{r}_0/c)dx_0dy_0, \quad \bar{r}_0 = x_0\hat{x}+y_0\hat{y} \tag{10}$$

which uses the time-domain near field directly. Assume for simplicity that we know the time derivative of the near field on the scan plane. (This is a realistic assumption because some probes actually measure the time derivative of the field [10].)

Equation (10) can be obtained by Fourier transforming the frequency-domain formula (2), which was converted to the double summation in (6) by means of the sampling theorem. Therefore, (10) can be converted to a summation by Fourier transforming (6) to get

$$\bar{\mathcal{F}}(\theta,\phi,t) = -\frac{1}{2\pi c}\hat{r}\times\sum_{m=-N_x}^{N_x}\sum_{n=-N_y}^{N_y}\hat{z} \times\frac{\partial}{\partial t}\bar{E}(\bar{r}_{0mn}, t+\hat{r}\cdot\bar{r}_{0mn}/c)\Delta x_0\Delta y_0 \tag{11}$$

where $\bar{r}_{0mn} = m\Delta x_0\hat{x} + n\Delta y_0\hat{y}$ is a sampling point on the scan plane and $\Delta x_0 = \Delta y_0 = \lambda_{min}/2$. This formula represents a time-domain sampling theorem that requires one to sample the time-domain near field at a spatial sample spacing of $\lambda_{min}/2$, the same spacing required by the frequency-domain computation scheme.

The direct time-domain formula (11) reveals a useful property of the time-domain computation scheme. If the source is turned on at $t = t_0$, one can calculate the far-field pattern for times $t < t_1$ by measuring the near field only for $t < t_2$. (This is not true for the frequency-domain computation scheme because the calculation of the frequency-domain near field requires the values of the time-domain near field over its entire duration.) To determine t_2 as a function of t_1 and the angle of observation θ, we assume that the scan plane is large enough that the near field has not reached its edges at $t = t_2$. Because the source is turned on at $t = t_0$, the near field $\bar{E}(\bar{r}_0, t)$ is zero for $|\bar{r}_0| > c(t-t_0)$ when $\bar{r}_0$ is far from the source region such that the minimum distance from the source region to $\bar{r}_0$ is approximately $|\bar{r}_0|$. From the time-domain formula (11), it is then seen that the latest time t_2 required to calculate the far-field pattern at the angle of observation θ and time t_1 is approximately given by $t_2 \simeq t_1 + |\bar{r}_{0max}|c^{-1}\sin\theta$, where $|\bar{r}_{0max}|$ is the radius of the circle in the scan plane circumscribing the nonzero near field at $t = t_2$. Consequently, $|\bar{r}_{0max}| = c(t_2 - t_0)$, and it is found that $t_2 \simeq \frac{t_1-t_0}{1-\sin\theta} + t_0$. Therefore, to calculate the far-field pattern at an angle θ for $t_0 < t < t_1$ one has only to measure the near field for $t_0 < t < t_2$. In particular, if the far-field pattern is calculated on the z axis ($\theta = 0$), we have that $t_2 = t_1$, as can be seen immediately from the time-domain formula (11) since $\hat{r}\cdot\bar{r}_{0mn} \equiv 0$ on the z axis. Thus, in contrast to the frequency-domain computation scheme, the time-domain computation scheme can calculate the far-field pattern for early times from near-field data measured solely at early times.

To calculate the far field at the angles of observation (θ,ϕ) and time t from the formula (11), one must know the near field at the point $\bar{r}_{0mn}$ on the scan plane at the time $\tau_{mn}(\theta,\phi) = t + m\Delta t\cos\phi\sin\theta + n\Delta t\sin\phi\sin\theta$ where $\Delta t = c^{-1}\Delta x_0 = c^{-1}\Delta y_0 = \pi/\omega_{max}$. Similarly, to calculate the far field at the angles of observation (θ',ϕ') and time t one must know the near field at the point $\bar{r}_{0mn}$ at the time $\tau_{mn}(\theta',\phi')$. The time difference $|\tau_{mn}(\theta,\phi)-\tau_{mn}(\theta',\phi')|$ for the two different angles of observation can be smaller than Δt, and therefore, in general, one needs the value of the near field at each $\bar{r}_{0mn}$ at times that lie between time samples with spacing Δt. However, since the near field is bandlimited, the standard sampling theorem shows that it is sufficient for reconstruction to sample the near field with time-sample spacing given by $\Delta t = \pi/\omega_{max} = \lambda_{min}/(2c)$. Assuming this has been done, the reconstruction theorem [5, p. 83] shows that the near field can be calculated at an arbitrary time t from the summation

$$\frac{\partial}{\partial t}\bar{E}(\bar{r}_{0mn},t) = \sum_{p=-\infty}^{+\infty}\frac{\sin(\pi(t/\Delta t-p))}{\pi(t/\Delta t-p)}\frac{\partial}{\partial t}\bar{E}(\bar{r}_{0mn},p\Delta t). \tag{12}$$

As in the previous section, we assume that the time-domain near field is significant only in the time interval $t_0 < t < t_0 + (N_\omega - 1)\Delta t$, where t_0 may depend on the position $\bar{r}_{0mn}$. Then the summation (12) becomes

$$\frac{\partial}{\partial t}\bar{E}(\bar{r}_{0mn},t) = \sum_{p=0}^{N_\omega-1}\frac{\sin\left[\pi\left(\frac{t-t_0}{\Delta t}-p\right)\right]}{\pi\left(\frac{t-t_0}{\Delta t}-p\right)} \cdot\frac{\partial}{\partial t}\bar{E}(\bar{r}_{0mn},t_0+p\Delta t) \tag{13}$$

where N_ω is the integer occurring in the frequency-domain formula (5). This reconstruction formula requires the calculation of N_ω values of the sinc function, N_ω real multiplications, and N_ω real additions. The reconstruction calculation must be performed for a number of time values depending on the far-field points, and at every near-field measurement point. Consequently, if N_ω is large, it may require a considerable amount of computer time.

However, for practical applications it may not be necessary to use the exact reconstruction formula (13). Instead one may be able to calculate the near field at a time t between the two time-sample points $p\Delta t$ and $(p+1)\Delta t$ by using the linear approximation formula

$$\frac{\partial}{\partial t}\bar{E}(\bar{r}_{0mn},t) = \frac{1}{\Delta t}\left\{[(p+1)\Delta t - t]\frac{\partial}{\partial t}\bar{E}(\bar{r}_{0mn},p\Delta t) +[t-p\Delta t]\frac{\partial}{\partial t}\bar{E}(\bar{r}_{0mn},(p+1)\Delta t)\right\}. \tag{14}$$

If this linear formula is inaccurate one can oversample, that is, let $\Delta t < \pi/\omega_{max}$, and then again use (14).

Assume that the linear approximation formula (14) can be used to accurately calculate the near field between time samples at times required by the far-field formula (11). Then it takes five real additions and three real multiplications to obtain the near field at each value of time between the time samples. On a typical computer (VAX 8650), the time it takes to perform one real multiplication is approximately 1.5 times larger than the time it takes to perform one real addition.

Therefore the calculation of the near field at a time between two time samples requires approximately the time it takes to perform ten real additions. Thus, the time it takes to calculate the full time-domain far-field pattern in (11) for $4N_xN_y$ far-field points and N_ω times is approximately equal to the time it takes to perform

$$A_f = 160N_\omega(N_xN_y)^2 \sim N_\omega(k_{max}r_s)^4 \tag{15}$$

real additions. Similarly, to calculate a principal-plane far-field cut (for example the $\phi = 0$ cut) requires the time it takes to perform

$$A_c = 80N_\omega N_x N_y^2 \sim N_\omega(k_{max}r_s)^3 \tag{16}$$

real additions. No complex multiplications are needed, and it is seen that the number of additions required to calculate a principal-plane far-field cut is significantly smaller than the number required to calculate the full far field.

Note from the expression (11) for the far-field pattern that if all fields are zero for $t < t_0$, the finite scan plane does not introduce any error into the far-field pattern calculation at times before the near field has reached the edges of the scan plane. This follows from the fact that $\bar{E}(\bar{r}_0, t) \equiv 0$ for $s > c(t - t_0)$, where s is the shortest distance from the source region to the point $\bar{r}_0$. In part C we show a numerical example that illustrates this property of the time-domain computation scheme. The formulas for the acoustic field can be obtained from the formulas of this section by replacing $\hat{z} \times \bar{E}$ with Φ, $\bar{\mathcal{F}}$ with $\mathcal{F}$, and $\hat{r}\times$ with $-\cos\theta$, respectively.

C. Comparisons of the Two Computation Schemes

We shall now compare and discuss the advantages and disadvantages of the frequency-domain computation scheme of part A of this section and the time-domain computation scheme of Part B. To compare the efficiency and convenience of the two schemes we start by using them to numerically calculate the far-field pattern of a simple acoustic antenna from near-field data taken on a square scan plane.

Acoustic point-source antenna: The acoustic point-source antenna is located at $\bar{r}_1 = -d\hat{z}$, $d > 0$, and its field is given by

$$\Phi(\bar{r}, t) = \frac{f(t - |\bar{r} - \bar{r}_1|/c)}{4\pi|\bar{r} - \bar{r}_1|} \tag{17}$$

where $f(t)$ is the Gaussian time function

$$f(t) = e^{-4t^2/\tau^2}, \quad f_\omega = \frac{\tau}{4\sqrt{\pi}}e^{-\omega^2\tau^2/16} \tag{18}$$

and τ equals half the signal width. The signal width 2τ is defined such that $|f(t)| < 0.02|f(0)|$ for $|t| > \tau$. Strictly speaking, this Gaussian pulse is not bandlimited. However, its spectrum is approximately zero for $\omega > 12/\tau$, and therefore the Gaussian pulse (18) can be approximated by a pulse that is bandlimited with a bandlimit given by $\omega_{max} = 12/\tau$. One finds that this general Gaussian signal, no matter how wide a bandwidth it has, can be reconstructed quite accurately from ten time samples [4, sec. 4.3].

With the bandlimit $\omega_{max} = 12/\tau$ it is found that $\lambda_{min} = 2\pi c/\omega_{max} \simeq c\tau/2$, and thus the spatial sample spacing is $\Delta x_0 = \Delta y_0 = \lambda_{min}/2 \simeq c\tau/4$. The point source is located at $\bar{r}_1 = -d\hat{z}$, where $d = 2\lambda_{min} \simeq c\tau$, and the scan plane is taken to be a square of sidelength $10d$ located in the plane $z = 0$.

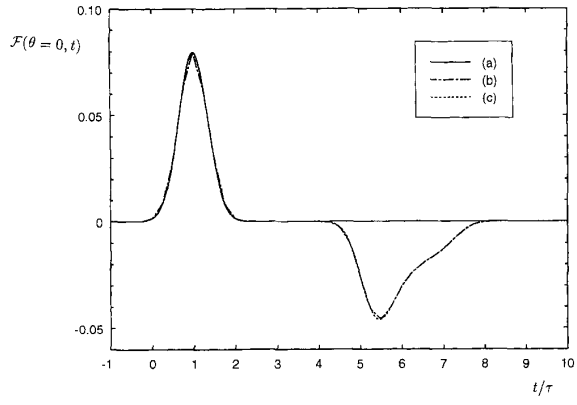

Fig. 2. On-axis far-field patterns for a Gaussian point source calculated with the time-domain computation scheme. (a) exact; (b) $\Delta t = \pi/\omega_{max}$; (c) $\Delta t = \pi/(3\omega_{max})$.

We start by showing results for the on-axis far-field pattern $\mathcal{F}(\theta = 0, t)$ obtained from the acoustic versions of the time-domain formula (11) and the linear approximation formula (14). Fig. 2 shows the following three plots of the on-axis far-field pattern $\mathcal{F}(\theta = 0, t)$: (a) the exact value, (b) the value obtained from the acoustic versions of (11) and (14) with $\Delta t = \pi/\omega_{max}$ (as prescribed by the standard sampling theorem), and (c) the value obtained from the acoustic versions of (11) and (14) with $\Delta t = \pi/(3\omega_{max})$ (that is, a value obtained by over sampling in time).

The first curve (a), which is exact, has the Gaussian waveform and is only significantly nonzero on the interval $-0.1\tau < t < 2.1\tau$. The second curve (b), which is obtained by using the standard time sample spacing $\Delta t = \pi/\omega_{max}$ and the linear approximation formula (14), has some visible discontinuities in its slope and approximates the exact curve well on the interval $-\tau < t < 4\tau$. On the interval $4\tau < t < 8\tau$ it is negative and erroneous. The third curve (c), which is obtained by over sampling with $\Delta t = \pi/(3\omega_{max})$ and using (14), cannot be distinguished from the exact curve on the interval $-\tau < t < 4\tau$ and is erroneous (like the second curve) on the interval $4\tau < t < 8\tau$. Before discussing the erroneous behavior of the two approximate curves (b) and (c) over this late-time interval, we note that by over sampling with $\Delta t = \pi/(3\omega_{max})$ one can use the simple linear approximation formula (14) to obtain an excellent approximation to the exact curve.

The erroneous behavior of the two approximate curves (b) and (c) on the interval $4\tau < t < 8\tau$ can be explained by first noting that the time integral of the expression (11) from $t = -\infty$ to $t = +\infty$ is zero for finite (truncated) scan planes because $\Phi(t = -\infty) = \Phi(t = +\infty) = 0$. This means that for the far-field patterns approximated by the summation in (11), $\int_{-\infty}^{+\infty} \mathcal{F}(\theta = 0, t)dt = 0$ which, of course, is not the case for the exact non-negative Gaussian far-field pattern. The integral representation [1, (76)] of the far-field pattern is exact, and since the near field is sampled with spacing of $\lambda_{min}/2$ (as required by the near-field sampling theorem [7]), we conclude

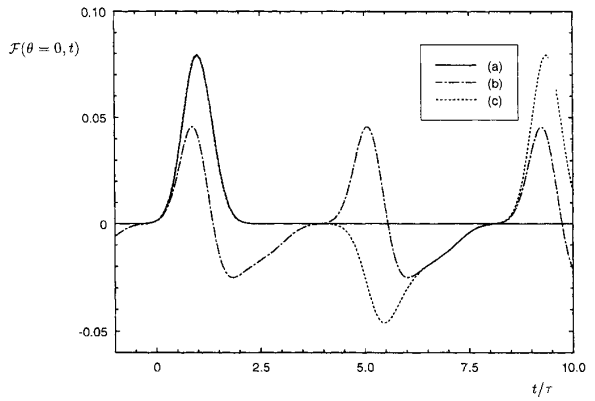

Fig. 3. On-axis far-field patterns for a Gaussian point source calculated with the frequency-domain computation scheme. (a) exact; (b) $N_\omega = 16$; (c) $N_\omega = 32$.

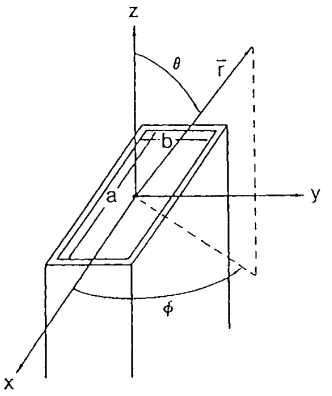

Fig. 4. Open-ended waveguide antenna.

that the erroneous behavior of the two approximate curves is due to the finite scan plane. This observation is confirmed by the fact that the time between the arrival of the direct signal ($t \simeq -0.1\tau$) and the arrival of the erroneous signal ($t \simeq 4.1\tau$) is equal to the time it takes the signal to travel the distance $l_1 - d$, where $l_1 = \sqrt{26}d$ is the distance from the source to the midpoint of the edges of the scan plane (recall that $\tau \simeq d/c$). Similarly, the time difference between the end of the direct signal ($t \simeq 2.1\tau$) and the end of the erroneous signal ($t \simeq 8\tau$) is the time it takes the signal to travel the distance $l_2 - d$, where $l_2 = \sqrt{51}d$ is the distance from the source to the corners of the scan plane.

Thus, the erroneous parts of the approximate far-field patterns are due to the fact that the scan plane is finite and represents diffraction from the artificial edges of the truncated scan plane. By enlarging the scan plane, the erroneous part of the approximate far-field pattern will move to later times, but it will never disappear when the scan plane is finite. Furthermore, from the exact integral [1, (76)] it is seen that for $t < 4\tau$ there is no contribution from the region outside the square scan plane with sidelength $10d$. Thus, for early times the truncated scan plane does not introduce any error into the calculation of the far-field pattern because the signal has not yet reached the edges of the scan plane. However, as time gets larger the signal reaches these edges and the finite scan plane introduces an error which is separated in time from the exact far-field pattern as demonstrated above.

This simple example shows that by over sampling in time one may avoid using the time consuming reconstruction formula (13) and instead use the simple linear approximation (14). Furthermore, it shows that the errors due to the finite scan plane are separated in time from the exact far-field pattern and can therefore be eliminated when using the direct time-domain computation scheme.

Having shown and discussed results obtained from the time-domain computation scheme, we now turn to the frequency-domain computation scheme. As explained in part A of this section, the frequency sample spacing $\Delta\omega = 2\omega_{max}/N_\omega$ for this scheme depends on the bandwidth ω_{max} of the near field and on the duration of the far field. Moreover, we have just shown that the duration of the far field is erroneously extended beyond that of the near field by the truncation of the scan plane. Thus, in practice, the required frequency sample spacing $\Delta\omega = 2\omega_{max}/N_\omega$ depends not only on the bandwidth ω_{max} (and the duration of the near field) but on the size of the scan plane.

From Fig. 2, showing the far-field pattern calculated from the time-domain computation scheme, it is seen that with our chosen scan-plane size the duration of the calculated time-domain far-field pattern is $T_f = 8.2\tau$, and therefore to avoid significant time-domain aliasing one must chose $\Delta\omega = 2\pi/T_f = 0.77\tau^{-1}$. This means that the number of time samples needed to avoid significant time-domain aliasing is $N_\omega = 2\omega_{max}/\Delta\omega \simeq 32$.

Fig. 3 shows the following three plots of the on-axis time-domain far-field pattern $\mathcal{F}(\theta = 0, t)$ calculated with the frequency-domain calculation scheme: (a) the exact value, (b) the value obtained from the acoustic versions of the frequency-domain formulas (5)–(7) with $N_\omega = 16$ (which is sufficient for reconstructing the near-field pulse), and (c) the value obtained by using the acoustic versions of (5)–(7) with $N_\omega = 32$ (the number prescribed by the sampling theorem to compute the far field extended in time by the truncated scan plane). The exact Gaussian curve (a) is only significantly nonzero on the interval $-0.1\tau < t < 2.1\tau$. The second curve (b) is periodic with period $T = \pi N_\omega/\omega_{max} = 4.2\tau$ and is clearly erroneous due to time-domain aliasing. The third curve (c) is periodic with period $T = 8.4\tau$ and cannot be distinguished from the exact curve (a) on the interval $-0.5\tau < t < 4.1\tau$. No significant time-domain aliasing occurs for the curve (c), and from Fig. 2 it is seen that curve (c) is simply a periodic repetition of the far-field pattern calculated from the time-domain computation scheme. Consequently, it has now been demonstrated that the frequency-domain computation scheme produces the same field as the time-domain computation scheme when the frequency sample spacing $\Delta\omega$ is chosen small enough to avoid time-domain aliasing caused by the field diffracted at the edges of the finite scan plane.

Open-ended waveguide antenna: Let us now consider the more complicated electromagnetic antenna consisting of an

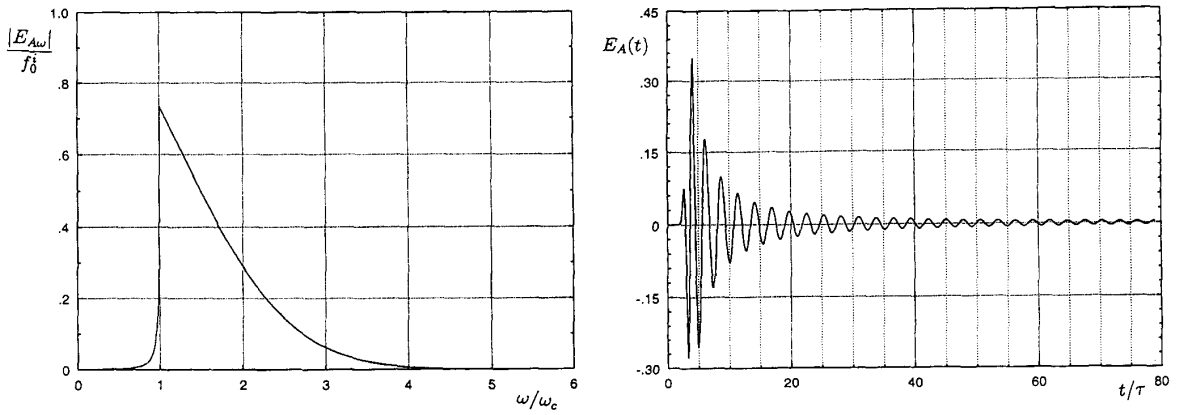

Fig. 5. Amplitude of spectrum and time dependence of aperture electric field for open-ended waveguide antenna.

open-ended rectangular waveguide fed by a source that has time dependence $f^i(t)$ and is located at the point $(x, y, z) = (0, 0, -d)$ in the waveguide shown in Fig. 4.

Assuming that the source is such that only the TE_{10} mode is excited, the part of the electric waveguide field that propagates in the direction of the positive z axis is given by

$$\bar{E}_{10}(\bar{r}) = \hat{y} f_\omega^i \cos\left(\frac{\pi x}{a}\right) e^{ik_z z} \tag{19}$$

where the longitudinal propagation constant is

$$k_z = \begin{cases} ik\sqrt{\left(\frac{\omega_c}{\omega}\right)^2 - 1}, & \omega < \omega_c \\ k\sqrt{1 - \left(\frac{\omega_c}{\omega}\right)^2}, & \omega > \omega_c \,. \end{cases} \tag{20}$$

Furthermore, $\omega_c = \pi c/a$ is the cutoff frequency for the TE_{10} mode and f_ω^i is the spectrum of the input signal. Note that the spectrum of the electric field is exponentially attenuated below cutoff and that its value at the center of the aperture is approximately given by

$$E_{A\omega} = \begin{cases} e^{-kd\sqrt{\left(\frac{\omega_c}{\omega}\right)^2 - 1}} f_\omega^i, & 0 < \omega < \omega_c \\ e^{ikd\sqrt{1 - \left(\frac{\omega_c}{\omega}\right)^2}} f_\omega^i, & \omega > \omega_c \,. \end{cases} \tag{21}$$

According to [11, (1) and (6)] the on-axis far-field pattern $\bar{\mathcal{F}}_\omega(\theta = 0)$ is given approximately by

$$\begin{aligned} \bar{\mathcal{F}}_\omega(\theta = 0) &= \mathcal{F}_\omega(\theta = 0)\hat{y} \\ &= C_0 \omega E_{A\omega} \left[1 + \Gamma + \frac{k_z}{k}(1 - \Gamma)\right] \hat{y} \end{aligned} \tag{22}$$

where C_0 is a frequency independent constant and Γ is a reflection coefficient that is approximately frequency independent over the recommended usable bandwidth of the waveguide.

Let us now calculate the time dependence of the aperture electric field and the on-axis far field for the special case where the source is Gaussian and the waveguide is X-band. In this case the TE_{10} cutoff frequency is $\omega_c = \pi c/a = 4.1 \cdot 10^{10}\ \mathrm{s}^{-1}$, $\Gamma \simeq 0.27 e^{i1.4}$, $a = 2.86$ cm, and $b = 1.016$ cm. The Gaussian source is chosen such that its spectrum, at the midpoint of the interval from ω_c to the next cutoff frequency $2\omega_c = 2\pi c/a = 8.2 \cdot 10^{10}\ \mathrm{s}^{-1}$, equals half its value at $\omega = 0$. Then the input pulse and its spectrum are given by (18), with $\tau = 5.4 \cdot 10^{-11}$ s. For $d = 5$ cm, the absolute value of the spectrum $E_{A\omega}$ and the time dependence $E_A(t)$ of the electric field at the center of the aperture are shown in Fig. 5.

It is seen from Fig. 5 that the spectrum for the aperture electric field is significantly attenuated below cutoff and that its slope is very large around the cutoff frequency. This spectrum is thus very different from that of the Gaussian input pulse because of the dispersion of the TE_{10} mode over the 5 cm of travel in the waveguide. The time dependence of the aperture electric field is also shown in Fig. 5 and is seen to be completely different from the Gaussian input pulse (18). In particular, the aperture electric field has a pulse width of approximately 80τ while the Gaussian input pulse has a pulse width of approximately 2τ. Since the bandwidth of the aperture field is the same as that of the input pulse, the time sample spacing for the signals are the same. This means that the number of time samples required for the aperture electric field is 40 times the number of time samples required for the Gaussian input pulse. It was mentioned above that the Gaussian input pulse required approximately ten time samples, so the aperture electric field requires approximately 400 time samples. In other words, to reconstruct the aperture electric field by use of the reconstruction theorem [5, p.83] one has to sample this field at 400 different times. And therefore, when a near-field to far-field calculation is performed for this near field, one must use 400 time samples to make sure that the far field is calculated accurately.

Let us now consider the far-field pattern (22), whose spectrum and time dependence are shown in Fig. 6. It is seen that the spectrum of the far-field pattern is very similar to that of the aperture electric field and that it is very different from the spectrum of the Gaussian input pulse. Near the cutoff frequency the spectrum of the far-field pattern is much smoother than the spectrum of the aperture electric field. The time dependence of the far-field pattern, also shown in Figure 6, is very similar to the time dependence of the aperture electric field. However, because of the smoother spectrum, the far-field pattern dies off faster with time than the aperture electric field and the pulse width of the far-field pattern is approximately 40τ, which is 20 times that of the input pulse.

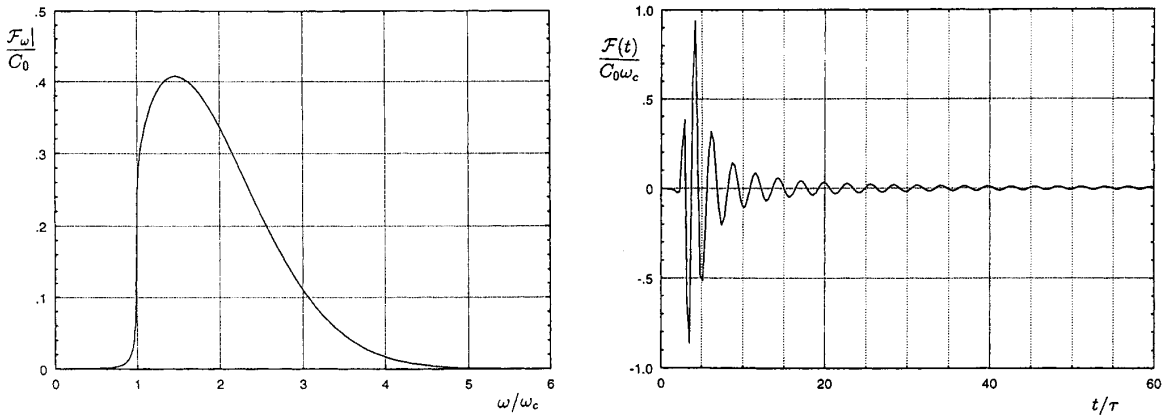

Fig. 6. Amplitude of spectrum and time dependence of on-axis far-field pattern for open-ended waveguide antenna.

In summary, for the open-ended waveguide antenna the time dependence of the aperture electric field and of the far-field pattern are very different from the time dependence of the input pulse because of the dispersive effects of the waveguide on the TE_{10} mode. In particular, for a Gaussian input pulse the time widths of the aperture electric field and far-field pattern are approximately 40 and 20 times larger than the time width of the input pulse, respectively. Assuming that the near field behaves as the aperture field, this means that one must measure the near field (at every near-field point on the scan plane) at approximately 400 different times when the waveguide is fed by a Gaussian pulse, which alone requires only ten time samples.

We will now discuss some of the consequences of using the two computation schemes to determine the far-field pattern of the open-ended waveguide. Assuming that the time dependence of the near field is similar to that of the aperture field shown in Figure 5, 400 near-field time samples are required to calculate the far-field pattern. (The open-ended waveguide antenna is directive, so it is assumed that the diffraction due to the edges of the scan plane is negligible.) The on-axis far-field pattern of the open-ended waveguide antenna, shown in Figure 6, consists of a main (early-time) part $(0 < t < 10\tau)$, which contains most of the power and an oscillatory part $(t > 10\tau)$. For some applications one may be interested only in the main part of the far-field pattern. From part B, it is found that the time-domain computation scheme can determine this early-time part of the on-axis far-field pattern from measured near-field data taken in the time interval $0 < t < 10\tau$. Since the duration of the near field is approximately 80τ (see Figure 5), only $\frac{1}{8} \cdot 400 = 50$ time samples are needed to calculate the main part of the far-field pattern using the time-domain computation scheme. Because the calculation of the frequency-domain near field requires the near field for its entire duration, the frequency-domain computation scheme needs all 400 time samples of the near field to calculate the main part of the far-field pattern. This example shows that if one is interested only in the far-field pattern for early times, the number of time samples of the near field required by the time-domain computation scheme can be much smaller than the number required by the frequency-domain computation scheme.

Computer time: Let us now compare the computer time required by the two computation schemes. For the far-field calculation performed in this section for the acoustic point-source antenna with Gaussian pulse excitation, the number of near-field sample points was $4N_xN_y = 1600$ because $N_x = N_y = 20$. To avoid time-domain aliasing caused by the edges of the scan plane, the number of time samples was $N_\omega = 32$ for the frequency-domain computation scheme (5)–(7), and therefore from (8) and (9) it is found that this scheme requires the calculation of $M_f = 5.3 \cdot 10^5$ and $M_c = 1.3 \cdot 10^5$ complex multiplications to compute the full far field and a principal-plane far-field cut, respectively. The on-axis result of this calculation is curve (c) of Fig. 3 and cannot be distinguished from the exact far field on the time interval where the exact far field is nonzero.

To perform the same far-field calculation for the acoustic point-source antenna using the time-domain computation scheme (11) with the linear time-approximation formula (14), two different values of N_ω were used, namely $N_\omega = 10$ (giving curve (b) of Fig. 2) and $N_\omega = 3 \cdot 10 = 30$ (giving curve (c) of Fig. 2). The far field obtained with $N_\omega = 10$ is a good approximation to the exact far field. The far field obtained with $N_\omega = 30$ cannot be distinguished from the exact far field on the time interval where the exact far field is nonzero. From (15) it then follows that $A_f = 2.6 \cdot 10^8$ and $A_f = 7.7 \cdot 10^8$ real additions are needed to calculate the full far field with ten and 30 time samples, respectively. Similarly, to calculate a principal-plane far-field cut $A_c = 6.4 \cdot 10^6$ and $A_c = 1.9 \cdot 10^7$, real additions are needed, using ten and 30 time samples, respectively.

Before comparing the results we note that on a typical computer (VAX 8650) the time it takes to perform one complex multiplication equals approximately six times the time it takes to perform one real addition. For the acoustic point-source antenna, we see that when the full far field is calculated, the frequency-domain computation scheme is by far the fastest because it makes use of the FFT. When only a principal-plane far-field cut is calculated the computation time for the time-domain computation scheme reduces significantly, whereas that of the frequency-domain computation scheme does not.

Next consider the open-ended X-band waveguide antenna fed by the Gaussian pulse with $\omega_{max} \simeq 4\omega_c = 1.6 \cdot 10^{11}$ s^{-1}. The scan plane is taken to be a square of sidelength 20 cm. Since $\lambda_{min} = 2\pi c/\omega_{max} = 1.1$ cm, we find that $N_x = N_y = 18$ and that the total number of near-field scan points is $4N_xN_y = 1296$. From the duration of the aperture field and the time-sample spacing, it follows that the number of near-field time samples is $N_\omega = 400$.

With these values of N_x, N_y, and N_ω one finds from (8) and (9) that the frequency-domain computation scheme requires $M_f = 7.1 \cdot 10^6$ and $M_c = 2.2 \cdot 10^6$ complex multiplications, respectively, to calculate the full far field and a principal-plane far-field cut. Similarly, the formulas (15) and (16) show that the time-domain computation scheme requires $A_f = 6.7 \cdot 10^9$ and $A_c = 1.9 \cdot 10^8$ real additions, respectively, to calculate the full far field and a principal-plane far-field cut.

Again, when the full far field is calculated, the frequency-domain computation scheme is by far the fastest, while the difference in computer time for the calculation of a principal-plane far-field cut is small. Furthermore, as discussed above, if one is interested only in calculating the far field for early times, the number of time samples required by the time-domain computation scheme reduces significantly, whereas that of the frequency-domain computation scheme does not. Thus, when only the early part of the far field is needed the time-domain scheme becomes more attractive.

In summary, when far fields are calculated for all times and all angles of observation, the FFT makes the frequency-domain computation scheme much faster than the time-domain computation scheme. When only part of the far field is calculated, the difference in computer time for the two computation schemes becomes smaller and the time-domain computation scheme becomes more advantageous because of its simplicity. In general, the time-domain computation scheme is much more direct and simpler than the frequency-domain computation scheme, and it does not have the problems of time-domain aliasing due to the finite scan plane. The time-domain computation scheme is much easier to use than the frequency-domain computation scheme, and it is consequently the more attractive scheme when one is not concerned with the amount of computer time it takes to perform the far-field calculations. Regardless of what computation scheme is used, planar time-domain near-field antenna measurements, unlike single-frequency near-field measurements [9], have the capability of eliminating finite scan errors. For some radiators, such as broadbeam antennas, this may be ample reason to consider time-domain measurements even when the final characterization of the radiator is required in the frequency domain.

REFERENCES

[1] T. B. Hansen and A. D. Yaghjian, "Planar near-field scanning in the time domain, part 1: Formulation," *IEEE Trans. Antennas Propagat.*, vol. 42, no. 9, pp. 1280–1291, Sept. 1994.

[2] ——, "Formulation of probe-corrected time-domain planar near-field measurements," Rome Laboratory In-House Rep. RL-TR-94-74, 1994.

[3] ——, "Formulation of probe-corrected planar near-field scanning in the time domain," *IEEE Trans. Antennas Propagat.*, in review.

[4] ——, "Formulation of time-domain planar near-field measurements without probe correction," Rome Laboratory In-House Rep., RL-TR-93-210, 1993.

[5] E. O. Brigham, *The Fast Fourier Transform and Its Applications*. Englewood Cliffs, NJ: Prentice, 1988.

[6] H. J. Nussbaumer, *Fast Fourier Transform and Convolution Algorithms*. New York: Springer, 1982.

[7] A. D. Yaghjian, "An overview of near-field antenna measurements," *IEEE Trans. Antennas Propagat.*, vol. AP-34, pp. 30–45, Jan. 1986.

[8] L. J. Kaplan *et al.*, "Rapid measurement and determination of antenna patterns using collapsed near-field data," in *Dig. Int. Symp. IEEE AP-S*, Stanford Univ., Stanford, CA, pp. 370–373, June 1977.

[9] M. L. Crawford, "Calibration of broadbeam antennas using planar near-field measurements," in *Dig. Conf. Precision Electromagnetic Measurements*, Boulder, CO, pp. 53–56, June-July 1976.

[10] M. Kanda, "Time domain sensors for radiated impulsive measurements," *IEEE Trans. Antennas Propagat.*, vol. AP-31, pp. 438–444, May 1983.

[11] A. D. Yaghjian, "Approximate formulas for the far field and gain of open-ended rectangular waveguide," *IEEE Trans. Antennas Propagat.*, vol. AP-32, pp. 378–384, Apr. 1984.

Thorkild B. Hansen (S'91–M'91), for a photograph and biography, please see p. 1402 of the November 1992 issue of this TRANSACTIONS.

Arthur D. Yaghjian (S'68–M'69–SM'84–F'92), for a photograph and biography, please see p. 312 of the March 1992 issue of this TRANSACTIONS.